










Rapid Aggregation of *Staphylococcus aureus* in Synovial Fluid Is Influenced by Synovial Fluid Concentration, Viscosity, and Fluid Dynamics, with Evidence of Polymer Bridging

 Amelia Staats,^{a,b}
 Peter W. Burback,^b
 Andrew Schwieters,^{a,b}
 Daniel Li,^c
 Anne Sullivan,^c
 Alexander R. Horswill,^d
 Paul Stoodley^{b,c,e}

^aDepartment of Microbiology, The Ohio State University, Columbus, Ohio, USA

^bDepartment of Microbial Infection and Immunity, The Ohio State University, Columbus, Ohio, USA

^cDepartment of Orthopaedics, The Ohio State University, Columbus, Ohio, USA

^dDepartment of Immunology and Microbiology, University of Colorado School of Medicine, Aurora, Colorado, USA

^eNational Centre for Advanced Tribology at Southampton, National Biofilm Innovation Centre, Department of Mechanical Engineering, University of Southampton, Southampton, United Kingdom

ABSTRACT Early bacterial survival in the postsurgical joint is still a mystery. Recently, synovial fluid-induced aggregation was proposed as a potential mechanism of bacterial protection upon entry into the joint. As synovial fluid is secreted back into the joint cavity following surgery, rapid fluctuations in synovial fluid concentrations, composition, and viscosity occur. These changes, along with fluid movement resulting from postoperative joint motion, modify the environment and potentially affect the kinetics of aggregate formation. Through this work, we sought to evaluate the influence of exposure time, synovial fluid concentration, viscosity, and fluid dynamics on aggregation. Furthermore, we aimed to elucidate the primary mechanism of aggregate formation by assessing the interaction of bacterial adhesins with the synovial fluid polymer fibrinogen. Following incubation under each simulated postoperative joint condition, the aggregates were imaged using confocal microscopy. Our analysis revealed the formation of two distinct aggregate phenotypes, depending on whether the incubation was conducted under static or dynamic conditions. Using a surface adhesin mutant, we have narrowed down the genetic determinants for synovial fluid aggregate formation and identified essential host polymers. We report here that synovial fluid-induced aggregation is influenced by various changes specific to the postsurgical joint environment. While we now have evidence that select synovial fluid polymers facilitate bridging aggregation through essential bacterial adhesins, we suspect that their utility is limited by the increasing viscosity under static conditions. Furthermore, dynamic fluid movement recovers the ability of the bacteria with surface proteins present to aggregate under high-viscosity conditions, yielding large, globular aggregates.

IMPORTANCE Infection is a major complication of knee and hip joint replacement surgery, which is used to treat arthritis or joint damage. We have shown that *Staphylococcus aureus*, a common bacterial pathogen, aggregates upon contact with synovial fluid. Within seconds, the bacterial cells interact with synovial fluid polymers in the joint fluid through their cell wall adhesins. The rapid formation of these aggregates likely aids in early bacterial survival in the joint, potentially contributing to the likelihood of developing an infection. By strengthening our basic understanding of the mechanics of synovial fluid aggregate formation under clinically relevant conditions, we hope to expand the knowledge of how to prevent or disrupt aggregation and reduce and more successfully treat these joint infections.

KEYWORDS surgical joint, synovial fluid, aggregation, orthopedics, *Staphylococcus aureus*, bacterial aggregates, biofilms, periprosthetic joint infection

Editor Jennifer M. Bomberger, University of Pittsburgh School of Medicine

Copyright © 2022 Staats et al. This is an open-access article distributed under the terms of the [Creative Commons Attribution 4.0 International license](https://creativecommons.org/licenses/by/4.0/).

Address correspondence to Paul Stoodley, paul.stoodley@osumc.edu.

The authors declare no conflict of interest.

This article is a direct contribution from Paul Stoodley, a Fellow of the American Academy of Microbiology, who arranged for and secured reviews by Robin Patel, Mayo Clinic, and Pradeep Singh, University of Washington School of Medicine.

Received 1 February 2022

Accepted 8 February 2022

Published 7 March 2022

In recent years, synovial fluid-induced aggregation of *Staphylococcus aureus* has been heavily investigated as a bacterial survival mechanism in the development of periprosthetic joint infections (PJIs). Numerous *in vitro* studies have provided novel insights into both the composition and pathogenic attributes of staphylococcal aggregates (1–5). It is now evident that aggregation occurs rapidly upon contact with synovial fluid and confers considerable recalcitrance to antibiotic administration (1, 3, 6, 7). To translate these hallmark findings to the clinic, it is critical that we first understand the primary mechanisms that mediate synovial fluid-induced aggregation, as well as how they are influenced by the postsurgical joint environment.

Bacterial aggregates have been observed existing both within the synovial fluid of chronically infected patients and recapitulated in the laboratory, often with the use of bovine synovial fluid (BSF), porcine synovial fluid, or equine synovial fluid (3, 8). In previous work, we demonstrated that synovial fluid-induced aggregation can be stimulated by individual components of synovial fluid, specifically fibrinogen and fibronectin (1). More recently, a synthetic synovial fluid composed of fibrinogen, hyaluronic acid, and albumin was shown to facilitate the formation of staphylococcal aggregates *in vitro* (4). These studies indicate that bacterial binding to host polymers within the synovial fluid plays a significant role in the development of synovial fluid-induced aggregates. However, it is still unclear how localized changes within the synovial joint in the context of surgery influence this process.

The synovial joint environment during and following surgery is highly dynamic, with several characteristics distinguishing it from a native joint. Following surgical site closure, invading bacteria encounter synovial fluid that is in compositional flux. The infiltration of blood into the joint dilutes the overall concentration of synovial fluid polymers that are suspected to facilitate aggregate formation (9). Furthermore, localized inflammation without indication of infection triggers a rapid influx of immune cells, leading to both protein degradation and hyaluronic acid cleavage (10–13). Hyaluronic acid, a glycosaminoglycan produced by resident synoviocytes, provides synovial fluid with its viscous property, which is essential for proper joint function (14–16). The breakdown of hyaluronic acid in the inflamed joint decreases the overall viscosity of the synovial fluid (17).

After a surgical procedure, the joint cavity is predominantly filled with blood. Over time, host cells lining the synovial membrane secrete synovial fluid back into the cavity, subsequently displacing the blood and changing the rheological properties of the fluid (9, 18). Together, the postsurgical joint becomes a complex system of shifting factors that potentially influence aggregation. We generated and tested several hypotheses based on current findings in the literature. Because synovial fluid-induced aggregation is dependent on binding to protein polymers within the fluid, we hypothesized that a compositional flux (e.g., a refilling postsurgical joint) would influence aggregate formation. We suspected that the addition of synovial fluid would enhance aggregation in a dose-dependent manner, with more circulating polymers providing a greater potential for bacterial bridging (19).

Following incubation in different concentrations of BSF, the average aggregate size and branch lengths were quantified using confocal microscopy followed by image analysis software. Because the overall viscosity changes over time due to both surgery-induced inflammation and synovial fluid infiltration, we next evaluated the influence of viscosity on aggregation, independent of increasing synovial fluid polymers. Finally, the postoperative synovial joint is seldom a static environment, with joint motion being encouraged immediately following surgery. Inducing joint flexion stimulates the movement of synovial fluid and blood in the joint, creating a dynamic environment (20). To investigate the effect of fluid dynamics and shear stress on the formation of synovial fluid aggregates, the bacteria were imaged macroscopically after incubation on either an orbital shaker or a rocker.

During our study, we noticed distinct phenotypic differences between aggregates formed under static and dynamic conditions. Because both conditions would likely exist at some point following surgical site closure, we wanted to understand the mechanics of aggregate formation under both conditions. With the use of a *S. aureus* quadruple surface adhesin mutant, AH4413 ($\Delta clfA \Delta fnbAB clfB::Tn$), we probed the necessity of fibrinogen and fibronectin-binding proteins under static incubation as well as on a shaker. Taken together, this work demonstrates that the

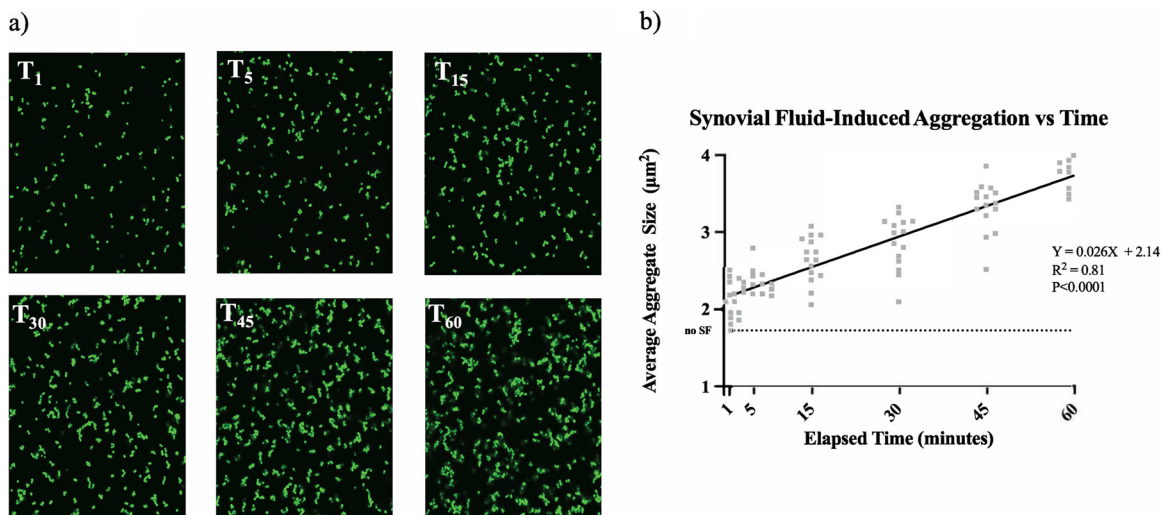


FIG 1 Aggregation of *Staphylococcus aureus* following contact with BSF. Confocal imaging of GFP-expressing *S. aureus* began immediately upon contact with BSF and continued for 1 h, with 5 representative images being captured at 0-, 1-, 5-, 15-, 30-, 45-, and 60-min time points (a). Fiji image analysis software was used to quantify the aggregate size at each point (b). To determine whether the relationship between time and aggregate size is statistically significant, a linear regression analysis was performed, as indicated by the black regression line. The dashed line indicates the average size of untreated bacteria after 1 h. Data points indicate 3 biological replicates.

unique characteristics of the postsurgical joint environment, including changes in fluid dynamics, synovial fluid concentrations, and viscosity, influence early aggregation, potentially contributing to the efficacy of synovial fluid-induced aggregation as a survival mechanism. Furthermore, we report evidence of a polymer bridging mechanism for aggregate formation, which requires the presence of specific bacterial surface adhesins.

RESULTS

Staphylococcal aggregates rapidly grow and adopt a branching phenotype over time following synovial fluid contact in a static system. We previously reported that *S. aureus* rapidly aggregates upon contact with BSF (1). With this preliminary knowledge, we first sought to validate our image-analysis-based method for quantifying aggregate size and branching. Throughout a 1-h incubation in BSF, 5 representative images of the aggregates were captured at various time points. Microscopy revealed a relative increase in aggregate size over time (Fig. 1a), with the average aggregate increasing by approximately $2 \mu\text{m}^2$ over 1 h (Fig. 1b). Time-lapse videos were collected in order to visualize the early kinetics of aggregate formation upon contact with phosphate-buffered saline (PBS) (see Movie S1 in the supplemental material), 10% BSF in PBS (see Movie S2), or 10% human serum in PBS (see Movie S3). Aggregate branching was also assessed to quantify aggregate morphology, which can differentiate mechanisms of polymer-mediated aggregation. Using image analysis software, we quantified the 50 longest aggregate branches at parallel time points throughout the 1-h incubation (Fig. 2a). Similar to aggregate size, branch length also correlated positively to BSF exposure time (Fig. 2b).

Synovial fluid induces an aggregate size threshold at high concentrations. Using our image analysis methodology, we next quantified aggregate size and branching as a function of various surgical joint-specific exposures. Previous studies showed that binding to protein polymers within the synovial fluid is essential for synovial fluid-induced aggregation of *S. aureus* to occur (4, 20). We hypothesized that increasing the synovial fluid concentration, and thus increasing the concentration of available bridging polymers, would facilitate the formation of larger aggregates with longer branches. As anticipated, we observed a relative increase in the average aggregate size after raising the synovial fluid concentration from 10% BSF to 20% BSF (Fig. 3a and b). Interestingly, increasing the concentration to 50% BSF resulted in reductions in both average aggregate size and branch length (Fig. 3c and d). These findings suggest that the increase in viscosity

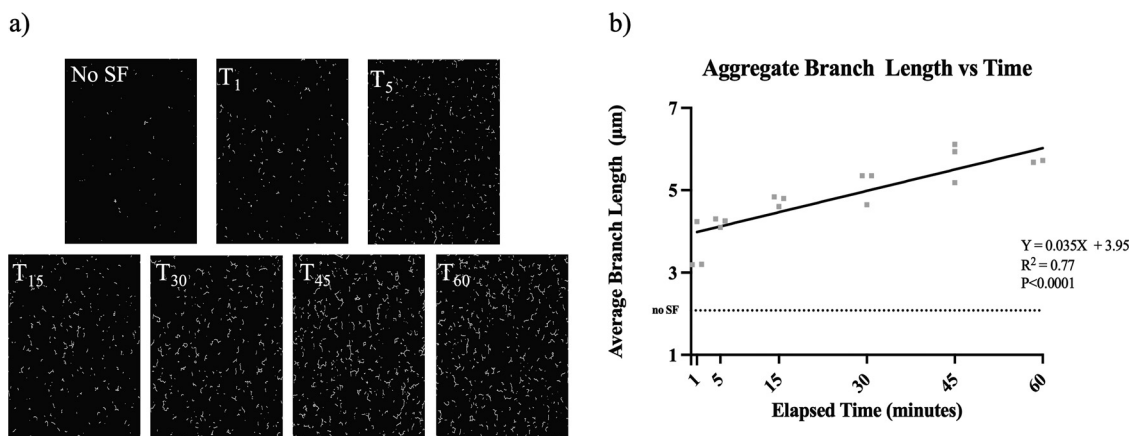


FIG 2 Branching analysis of *Staphylococcus aureus* following contact with BSF. Confocal imaging was conducted immediately upon contact with BSF (SF) and continued for 1 h, with 5 representative images being collected at 0-, 1-, 5-, 15-, 30-, 45-, and 60-min time points. Fiji image analysis software was used to skeletonize the aggregates for branching quantification (a). The average branch length of the 50 longest branches was calculated for each time point (b). To determine whether the relationship between time and branch length is statistically significant, a linear regression analysis was performed, as indicated by the black regression line. The dashed line indicates the average branch length of untreated bacteria after 1 h. Data points indicate the average of 3 biological replicates.

associated with the higher concentrations may inhibit synovial fluid polymer binding as well as interbacterial interactions.

Increasing solution viscosity with hyaluronic acid inhibits staphylococcal aggregation independent of synovial fluid protein polymers. To investigate the effect of an increasingly viscous joint space on synovial fluid-induced aggregate formation, various concentrations of purified, high-molecular-weight hyaluronic acid were supplemented into a baseline concentration of 10% BSF. Hyaluronic acid was chosen because it is the primary contributor to the viscous property of synovial fluid and does not stimulate staphylococcal aggregation independent of the other synovial fluid components at physiological concentrations (1). Prior to imaging studies, we measured the viscosity of the different synovial fluid concentrations and hyaluronic acid-supplemented synovial fluid using a rheometer. As we increased the concentration of synovial fluid in the solution, the viscosity increased in a dose-dependent manner (Fig. 4a). Similarly, supplementation with purified hyaluronic acid elevated the overall viscosity (Fig. 4b). Increasing the concentration of hyaluronic acid on top of the baseline 10% BSF decreased both the average size (Fig. 4c and d) of the aggregates and the length of the branches (Fig. 4e and f), indicating that viscosity plays a significant role in the extent of synovial fluid-induced aggregation.

Dynamic incubation of *S. aureus* in synovial fluid recovers aggregation at high synovial fluid concentrations. In addition to changes in synovial fluid viscosity and polymer composition within the postsurgical joint cavity, there is the introduction of fluid flow (20). Synovial fluid and blood flow within the enclosed space are stimulated by normal joint flexion as well as prescribed therapeutic flexion (21). To probe the influence of fluid dynamics on synovial fluid-induced aggregation of *S. aureus*, we incubated the bacteria statically, on an orbital shaker, or on a rocker for 1 h in various concentrations of BSF before macroscopic imaging. Under static conditions, macroscopic aggregates were not visible in the petri dishes (Fig. 5a). Under dynamic conditions, however, free-floating, globular aggregates were observed, even at high concentrations of synovial fluid (Fig. 5b). Macroscopic imaging was also conducted following incubation on a rocker, which we expect more closely resembles joint-flexion-induced fluid flow. Similar to the orbital shaker, the rocker yielded large aggregates; however, they were less globular in morphology (Fig. 5c). Finally, macroscopic aggregates were imaged after incubation in increasing concentrations of hyaluronic acid (Fig. 5d). These findings indicate that fluid dynamics can overcome the negative effect of viscosity on aggregation, as observed previously.

Fibronectin-binding proteins and clumping factors mediate rapid aggregation through a polymer bridging mechanism. Because the presence of fibrinogen and fibronectin is reportedly essential for bacterial aggregation in synovial fluid, we next sought to validate the importance of select microbial surface components recognizing adhesive

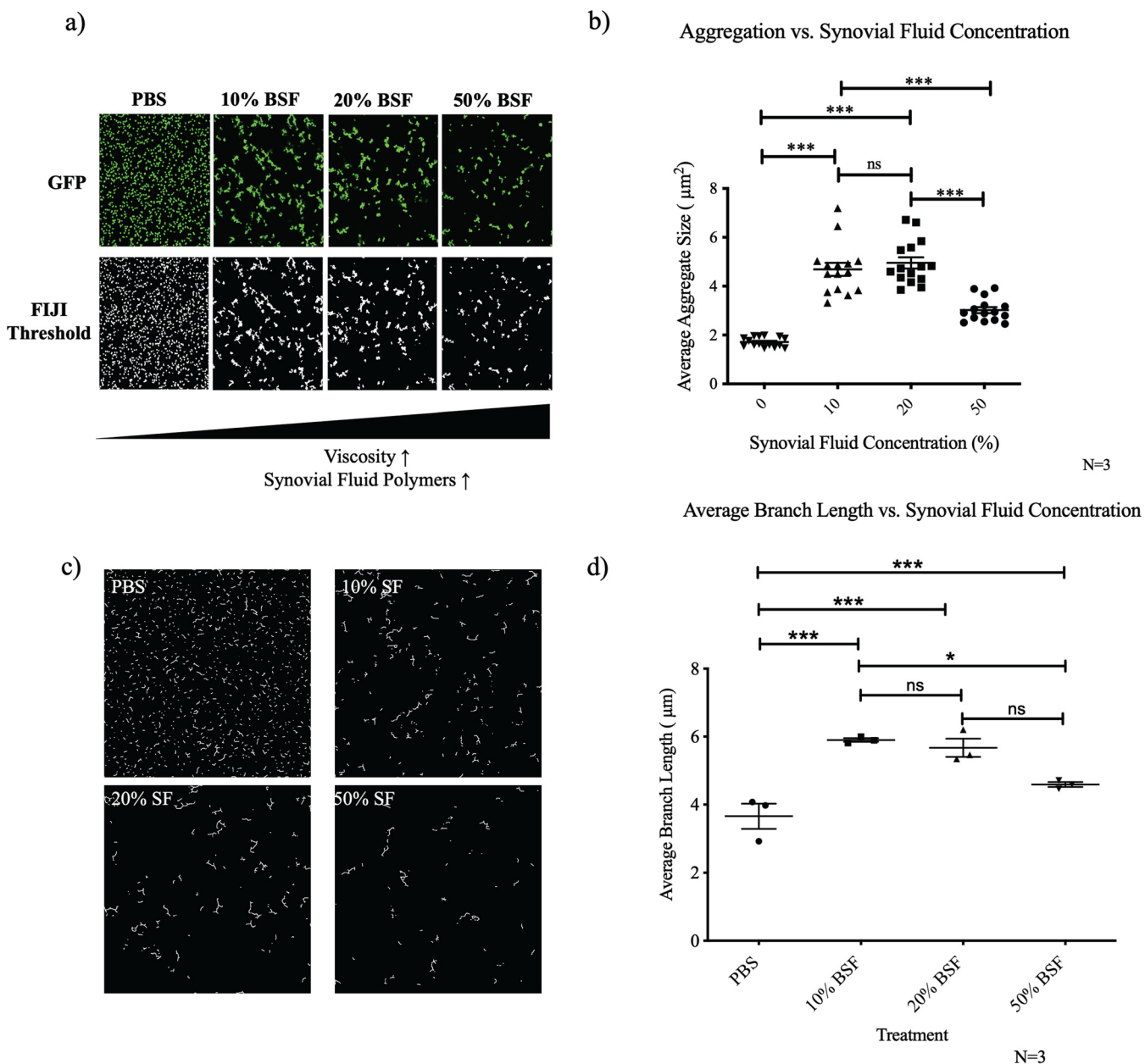


FIG 3 Increasing the concentration of BSF inhibits aggregation under static conditions. Synovial fluid (SF)-induced aggregates were imaged using confocal microscopy following 1 h of incubation in either PBS, 10% BSF, 20% BSF, or 50% BSF (a). Fiji image analysis software was used to quantify the average particle size (b). Images were skeletonized (c), and the average branch length of the 50 longest branches was calculated (d). Data points represent 3 biological replicates, with 5 representative images being collected for each replicate. Error bars indicate SEM. Statistical significance was determined by one-way ANOVA with Bonferroni's multiple-comparison test to compare means between treatments. ns, not significant ($P > 0.05$); *, $P \leq 0.05$; ***, $P \leq 0.001$.

matrix molecules (MSCRAMMs) using a *S. aureus* quadruple adhesin mutant strain ($\Delta clfA \Delta fnbAB clfB::Tn$). Following 1 h of static incubation in either PBS or 10% BSF in PBS, both the wild-type *S. aureus* strain and the adhesin mutant were imaged using confocal microscopy (Fig. 6a). While both strains were capable of forming phenotypically comparable branched aggregates, image analysis quantification revealed that the adhesin mutant formed significantly smaller aggregates, compared to those of the wild-type strain (Fig. 6b), with a higher degree of aggregate circularity (Fig. 6c). When incubated under dynamic conditions on an orbital shaker, the wild-type strain conglomerated into a macroscopic, free-floating aggregate, while the mutant strain remained dispersed throughout the petri dish (Fig. 6d).

We hypothesized that this defect was due to a lost interaction between one or more bacterial surface adhesins and the synovial fluid polymer. We repeated the experiment using

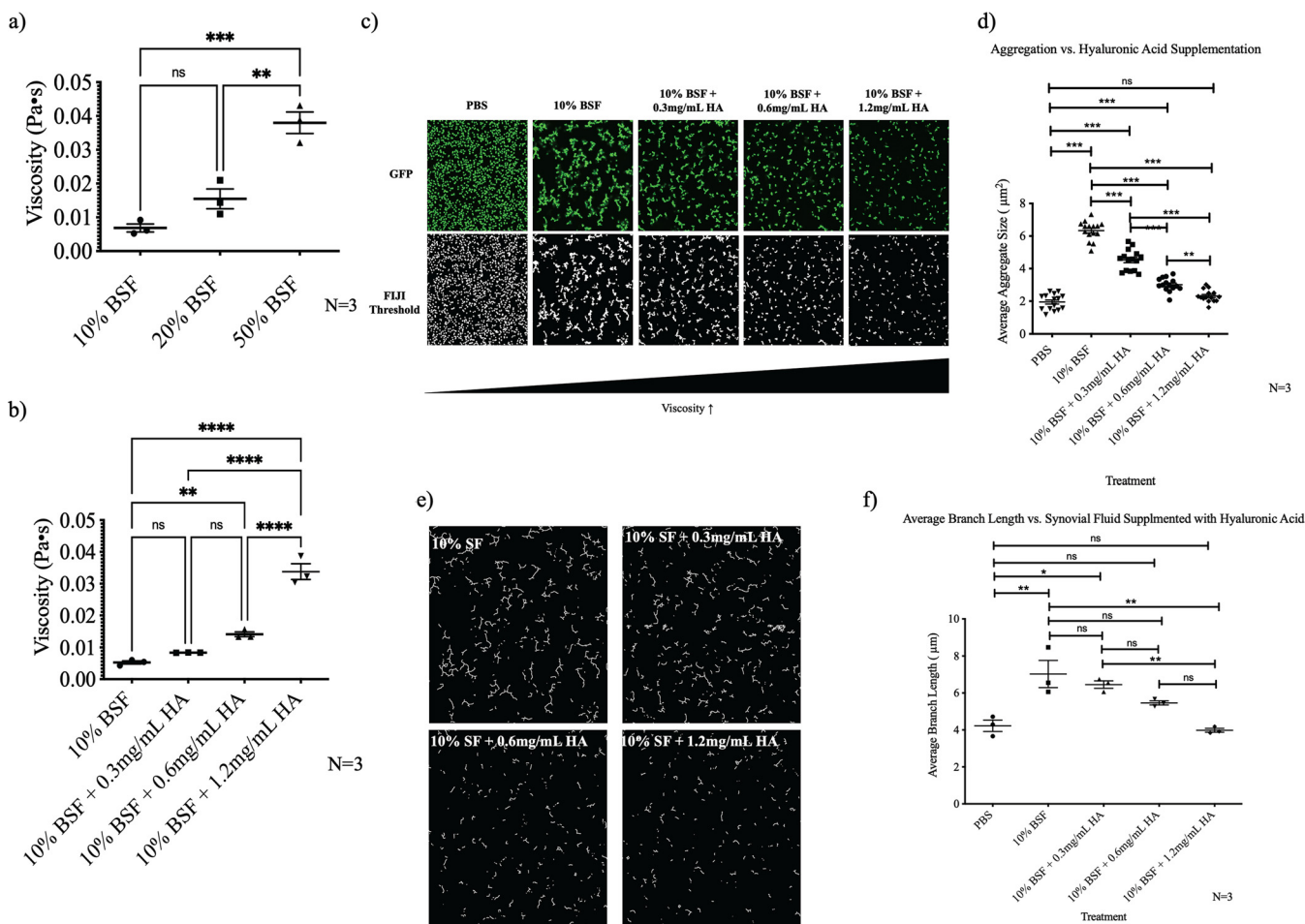


FIG 4 Increasing the solution viscosity inhibits synovial fluid (SF)-induced aggregation independent of increasing fibrinogen and fibronectin bridging polymers. A rheometer was used to measure the viscosity of increasing concentrations of BSF (a) and 10% BSF supplemented with increasing concentrations of hyaluronic acid (HA) (b). Synovial fluid-induced aggregates were imaged using confocal microscopy following 1 h of incubation in either PBS, 10% BSF, or 10% BSF supplemented with various concentrations of hyaluronic acid (c). Fiji image analysis software was used to quantify the average particle size (d). Images were skeletonized (e), and the average branch length of the 50 longest branches was calculated (f). Data points represent 3 biological replicates, with 5 representative images being collected for each replicate. Error bars indicate the mean \pm SEM. Statistical significance was determined by one-way ANOVA with Bonferroni's multiple-comparison test to compare means between treatments. ns, not significant ($P > 0.05$); *, $P \leq 0.05$; **, $P \leq 0.01$; ***, $P \leq 0.001$; ****, $P \leq 0.0001$.

purified Alexa Fluor-conjugated fibrinogen. Fibrinogen alone was selected because it was documented previously to play an important role in staphylococcal aggregation (1, 4). Similar to the 10% BSF, the wild-type strain formed a single, macroscopic, free-floating aggregate following 1 h of dynamic incubation on a shaker. Upon microscopic analysis, we visually observed strong fibrinogen colocalization. In contrast, the adhesin mutant was unable to form a free-floating aggregate under shear and displayed little interaction with the fibrinogen (Fig. 7a). Interestingly, under static conditions, the adhesin mutant was unable to form the branched aggregates that were still observed following static incubation in the 10% BSF (Fig. 7b).

Quantification through image analysis revealed that fibrinogen alone produced aggregates that were 2-fold larger than those of the untreated wild-type bacteria and 2-fold smaller than the 10% BSF aggregates (Fig. 7c). There was no significant difference between the untreated adhesin mutant and that treated with the fibrinogen (Fig. 7d). Experiments with the adhesin mutant revealed that mutations in select MSCRAMMs abolish the aggregate phenotype under dynamic conditions but not static ones. Statically stimulated aggregation of the mutant is ultimately lost when it is incubated with a single synovial fluid polymer, fibrinogen. Because the wild-type strain is still able to aggregate in fibrinogen alone, this suggests a direct role for fibrinogen in synovial fluid-induced aggregation, as well as an interaction, at the genetic level, between fibrinogen and one or more MSCRAMMs. Furthermore, the ability

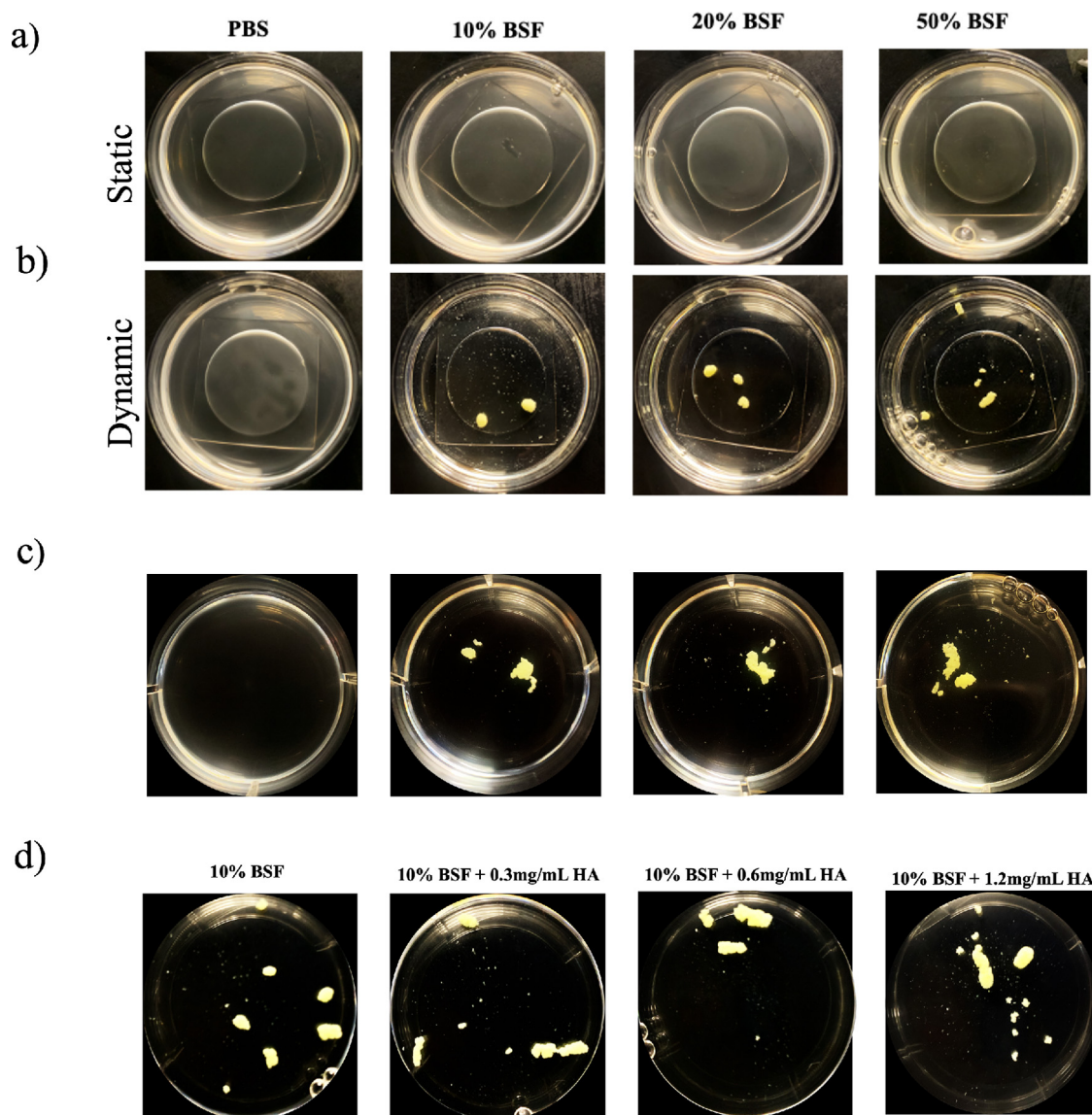


FIG 5 Dynamically incubating *Staphylococcus aureus* in BSF recovers aggregate formation at high concentrations of synovial fluid and in high-viscosity solutions. *S. aureus* was imaged following 1 h of incubation statically on a benchtop (a) or dynamically on an orbital shaker (b) or a rocker (c) with increasing concentrations of BSF. Additionally, macroscopic imaging was conducted following dynamic incubation on an orbital shaker with increasing concentrations of hyaluronic acid (HA) (d). Following a 1-h incubation, petri dishes were imaged macroscopically with a camera.

of the adhesin mutant to still aggregate statically in the 10% BSF but not the purified fibrinogen indicates that other polymers within the synovial fluid may be contributing independently to the branched phenotype.

To solidify our claim that synovial fluid-induced aggregation is mediated by a rapid bridging interaction between bacterial surface proteins and host polymers (as opposed to an active process), we conducted aggregation assays with antibiotic-treated bacteria. Following treatment with gentamicin, nonviable *S. aureus* was incubated in 10% BSF and assessed for aggregation. Confocal imaging revealed that, throughout a 1-h incubation, the dead bacteria were still able to aggregate in the 10% BSF (see Fig. S3a). These data indicate that the presence of the surface adhesins is sufficient to facilitate aggregate formation, further explaining the rapidity with which the bacteria come together upon synovial fluid exposure.

Dynamic bacterial aggregation becomes less efficient as synovial fluid displaces blood. As mentioned previously, blood predominantly occupies the joint cavity following surgical site closure. To mimic the influence of the transition from a blood-dominated cavity to a

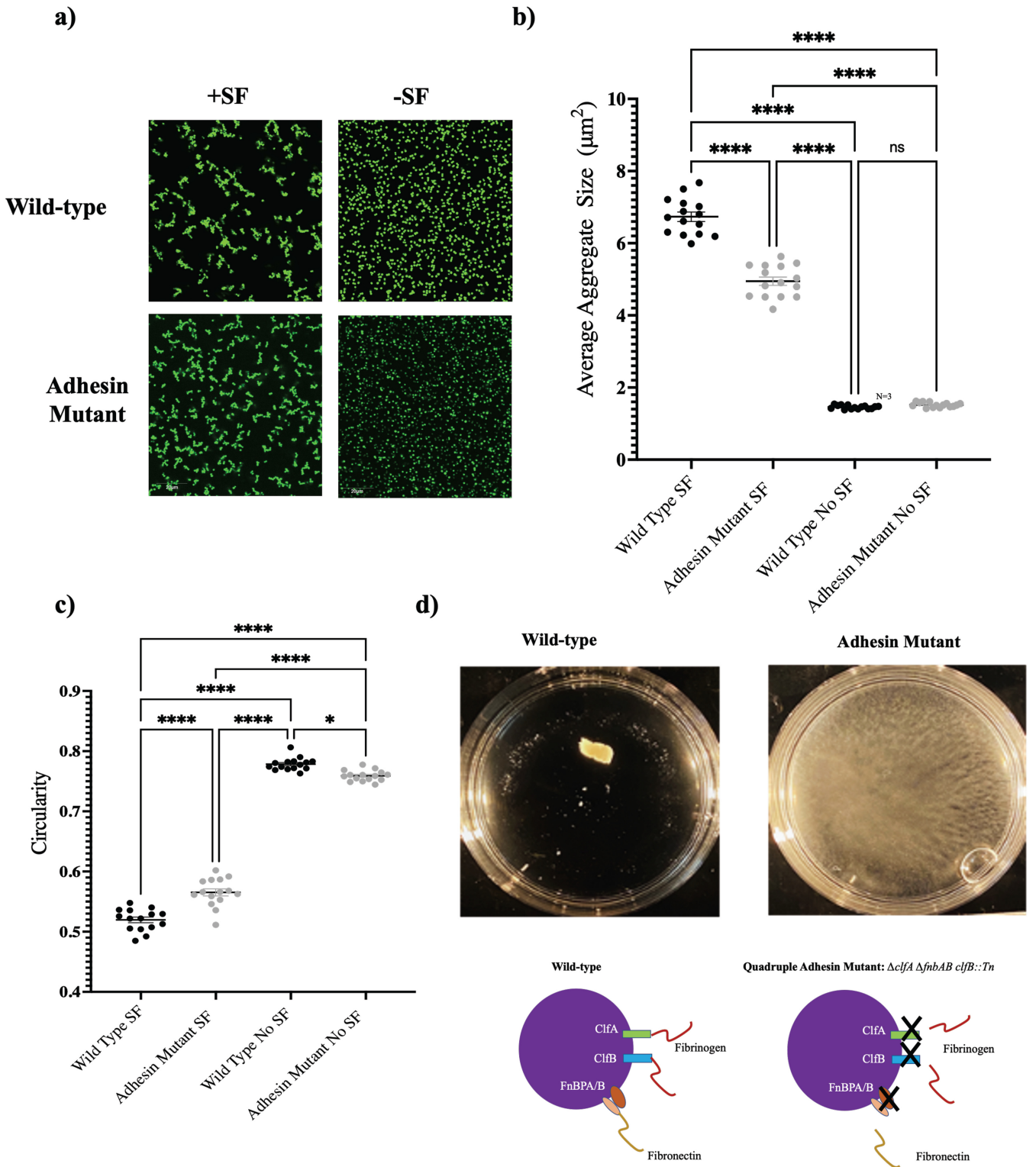


FIG 6 Key surface adhesins are essential for macroscopic aggregation under dynamic incubation but not required for the static formation of the microscopic branching aggregate phenotype. Wild-type *Staphylococcus aureus*, AH1263, and the quadruple adhesin mutant AH4413 ($\Delta\text{clfA } \Delta\text{fnbAB } \text{clfB}::\text{Tn}$) were incubated statically in 10% BSF (SF) or PBS before imaging with confocal microscopy (a). The average aggregate size (b) and circularity (c) were determined using Fiji image analysis software after 1 h of incubation. Following 1 h of dynamic incubation on an orbital shaker, the aggregates were imaged macroscopically (d). Data points represent 3 biological replicates, with 5 representative images being collected for each replicate. Error bars indicate the mean \pm SEM. Statistical significance was determined by one-way ANOVA with Bonferroni's multiple-comparison test to compare means between treatments. ns, not significant ($P > 0.05$). *, $P \leq 0.05$; ****, $P \leq 0.0001$.

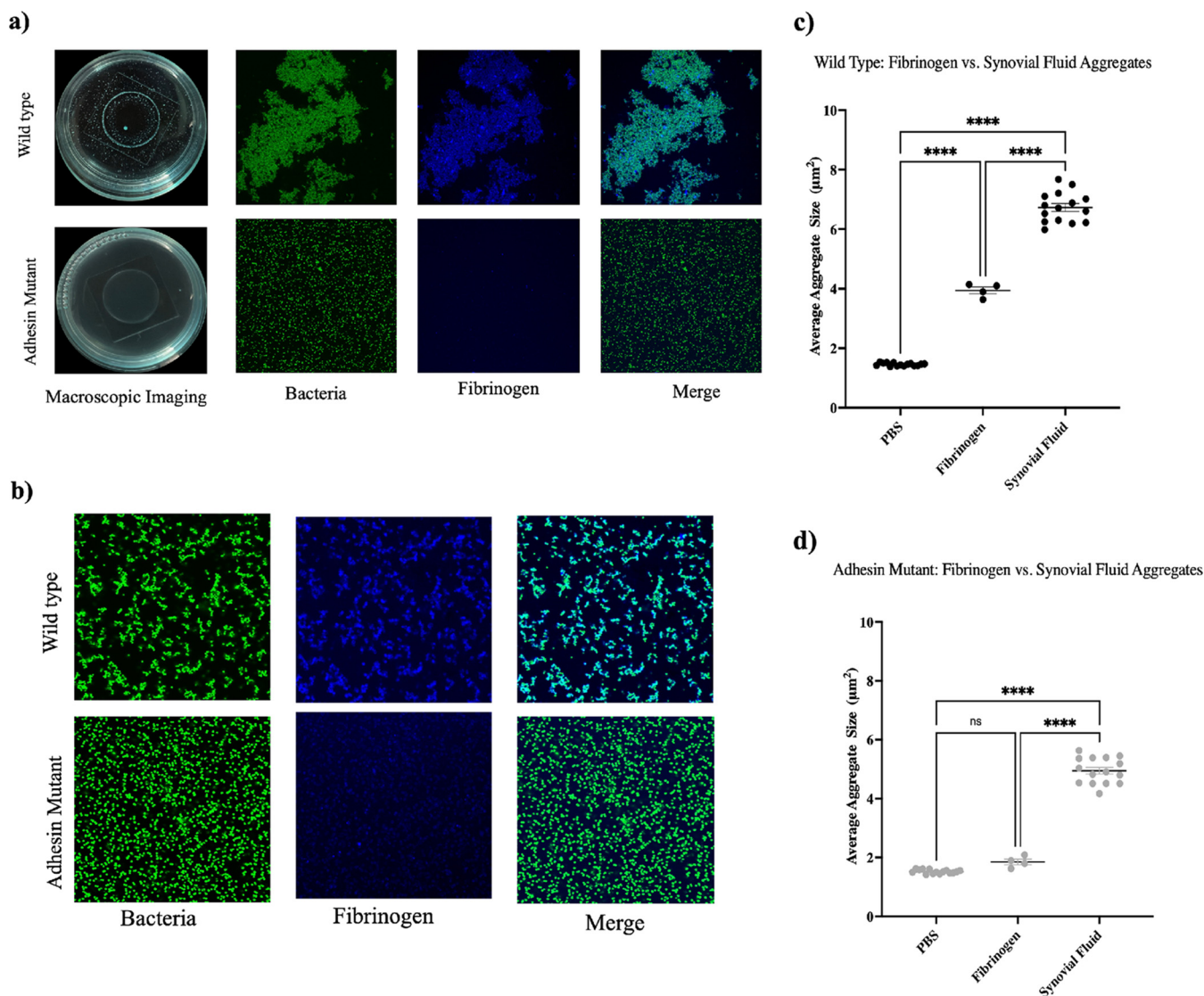


FIG 7 Polymer bridging aggregation is facilitated by direct interaction between bacterial surface adhesins and fibrinogen. Macroscopic and confocal microscopy images were captured of both wild-type *Staphylococcus aureus* and the quadruple adhesin mutant following 1 h of either dynamic (a) or static (b) incubation in Alexa Fluor-conjugated fibrinogen. Following static incubation, the average aggregate size was calculated for the wild-type strain (c) and the mutant (d). Error bars indicate the mean \pm SEM. Data points represent 3 biological replicates, with 5 representative images being collected for each replicate. Statistical significance was determined by one-way ANOVA with Bonferroni's multiple-comparison test to compare means between treatments. ns, not significant ($P > 0.05$); ****, $P \leq 0.0001$.

synovial fluid-dominated one, we conducted macroscopic imaging after 1 h of dynamic incubation in synovial fluid supplemented with human blood (Fig. 8a). Comparable aggregation was observed with the 100% blood condition and the combination of 90% blood with 10% BSF condition. Interestingly, at higher concentrations of BSF (<75%), macroscopic aggregation appeared dwarfed, with smaller bacterial aggregates and clusters forming. Confocal microscopy of the 10% BSF in blood was conducted to confirm that the observed aggregates were green fluorescent protein (GFP)-tagged staphylococcal aggregates (Fig. 8b).

DISCUSSION

Synovial fluid-induced aggregation of *S. aureus* is under investigation as a potential pathogenic survival mechanism in the occurrence of (PJIs). While a considerable amount of work characterizing this process has been conducted, until now the influence of surgical site-specific conditions on aggregate formation has been neglected. Following prosthetic joint surgery, numerous changes associated with inflammation and joint flexion occur. These changes

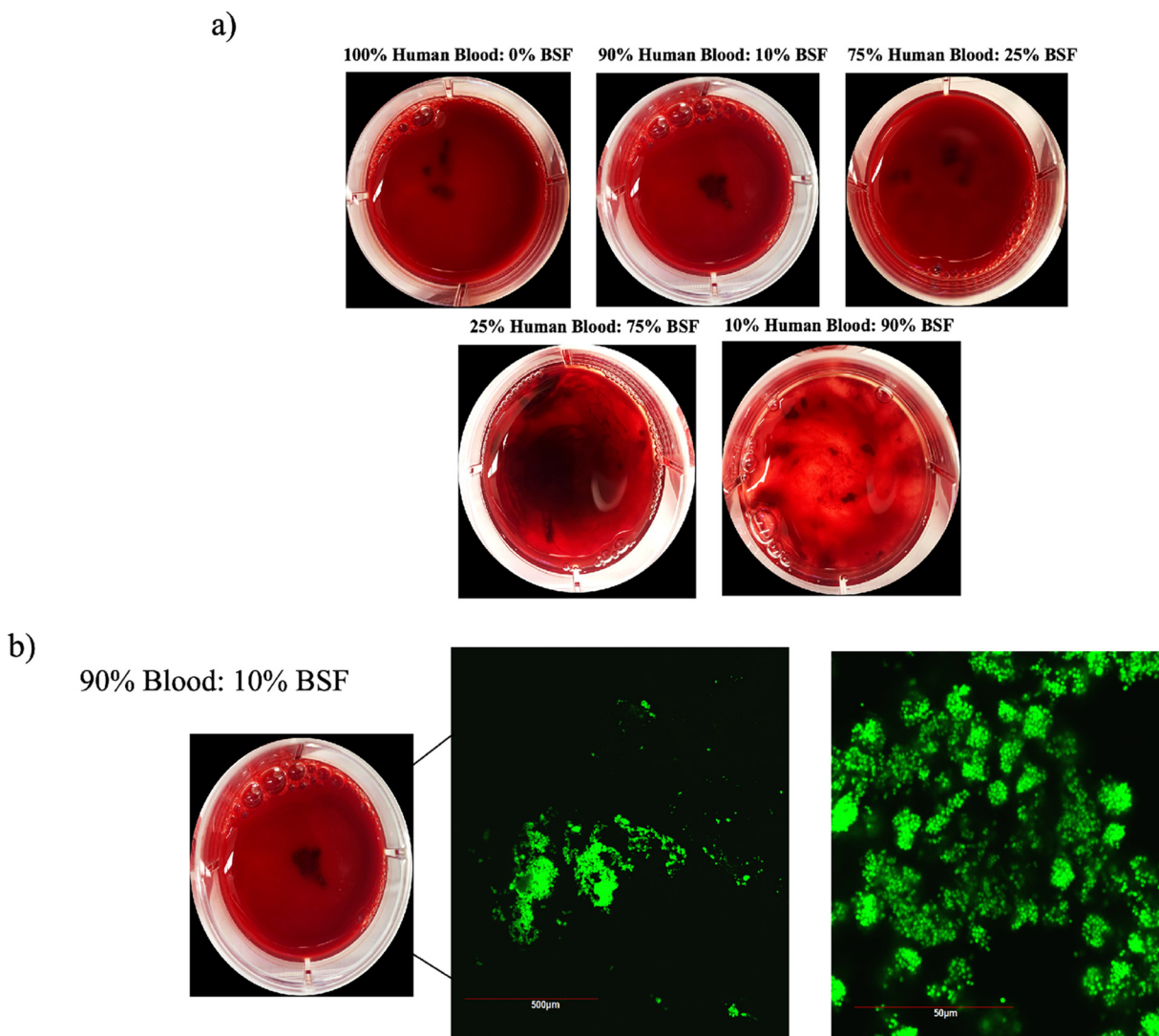


FIG 8 Dynamic incubation of *Staphylococcus aureus* in human blood supplemented with BSF. GFP-expressing *S. aureus* was incubated for 1 h in human blood supplemented with increasing concentrations of BSF. Macroscopic imaging of the petri plates was conducted for the free-floating aggregates (a), followed by confocal microscopy to validate the presence of bacteria in the aggregates (b).

are highly distinct from a native joint environment and should be taken into consideration when studying the establishment and progression of bacterial infections. Furthermore, analysis of synovial fluid-induced aggregates has been confined to long incubations (<90 min), leaving the initial kinetics of aggregation unclear.

We previously published work demonstrating that staphylococcal aggregation occurs rapidly upon contact with BSF. Using confocal microscopy, *S. aureus* was imaged immediately following exposure to either 10% BSF in PBS, 10% human serum in PBS, or PBS alone. Our videos reveal that not only does aggregation occur immediately upon contact with the BSF but also the resulting aggregates form distinctive branched structures as they develop. In contrast to tightly packed, globular bacterial clusters that form from polymer depletion, the branching structures we observed appear visually similar to those generated through diffusion-limited cluster aggregation (DLCA) and reaction-limited cluster aggregation (RLCA) (22). This model was developed from colloidal physics to explain the shape and growth of different structures formed from colloidal particles within a liquid. In this case, particles diffuse through a surrounding medium and stick together irreversibly whenever they collide (DLCA) or with a certain probability upon each collision (RLCA) (22).

Two dominating mechanisms of bacterial aggregation when either host-produced or bacterial polymers are present have recently been proposed (19). Depletion aggregation is an entropy-driven process in which high concentrations of nonadsorbing polymers constrain the bacteria together. This mechanism predominantly yields tightly packed bacterial aggregate arrangements due to spontaneous motion of the surrounding polymers, pushing the bacteria together and maximizing the space in which the polymers have to move (19). The second primary mechanism of polymer-induced aggregation is bridging aggregation, in which the host or bacterial polymers adsorb on the bacterial cells (19).

While synovial fluid is a complex host fluid composed of numerous polymers, we speculated that synovial fluid-induced aggregation of *S. aureus* is dominated by the bridging aggregation mechanism, with fibrinogen or fibronectin serving as bridging polymers (19). The highly branched morphology of the synovial fluid aggregates corroborates this theory, because bridging aggregation yields random bacterial arrangements due to the attachment of polymers interacting with various surface adhesins dispersed across the cell surface (19). In contrast, the human serum aggregates also grew over time but revealed less aggregation with fewer intricate branches. These results were expected because serum lacks fibrinogen and fibronectin polymers required for extensive bridging aggregation but still contains albumin at high concentrations, likely facilitating the observed clumping.

Based on our observations from the time-lapse microscopy of the initial kinetics, we hypothesized that aggregate size and branching would increase with the synovial fluid concentration. To assess the influence of various synovial fluid concentrations on aggregate formation, we incubated *S. aureus* for 1 h in PBS, 10% BSF in PBS, 20% BSF in PBS, and 50% BSF in PBS before confocal imaging. To our surprise, both aggregate size and branch length increased in a dose-dependent manner with the synovial fluid concentration up to the 50% BSF treatment. Although the amount of available bridging polymers increases with the synovial fluid concentration, the overall viscosity of the solution also increases. These results suggest that a threshold exists at which the synovial fluid is too viscous for interbacterial interaction. We suspect that, once this threshold is reached, even an abundance of fibrinogen and fibronectin cannot recover the larger aggregates under static conditions. These data indicate that the early time points following surgical site closure, when the blood-to-synovial fluid ratio is higher, may facilitate the optimal conditions for staphylococcal aggregate formation.

To probe our theory that a viscosity-induced threshold for aggregation exists at higher concentrations of synovial fluid, we quantified both aggregate size and branching following incubation in 10% BSF supplemented with increasing concentrations of high-molecular-weight hyaluronic acid sodium salt. The addition of hyaluronic acid increased the viscosity of the solution dose-dependently and inhibited aggregation of *S. aureus* independent of increasing concentrations of synovial fluid protein components. We acknowledge that the use of hyaluronic acid as an agent for viscosity manipulation introduces a confounding variable into our system. However, previous studies in our laboratory showed that hyaluronic acid alone does not stimulate staphylococcal aggregation at the applied concentrations (1).

While a static synovial joint environment may closely mimic the immediate conditions following surgical site closure, most surgeons advise patients to introduce movement as part of a standard postoperative protocol (21). Patients not only are fully weight-bearing after surgery but also are encouraged to partake in physical therapy to maintain a full range of motion, including maximal knee flexion. Induced synovial fluid movement introduced postoperatively likely creates a highly interactive environment, enhancing interbacterial interaction as well as increased contact with circulating synovial fluid polymers. With the use of an orbital shaker, we incubated *S. aureus* dynamically for 1 h in either PBS, 10% BSF in PBS, 20% BSF in PBS, or 50% BSF in PBS. Macroscopic imaging revealed the presence of large, free-floating aggregates, even at the higher concentrations of BSF. These findings suggest that dynamic synovial fluid movement recovers the ability of the bacteria to aggregate under conditions of high viscosity, because it facilitates a greater degree of bacterial interaction with each other and with the bridging polymers. We also conducted dynamic aggregation experiments on a

rocker, because the motion more closely resembles the back-and-forth movement stimulated by joint flexion (20). While the rocker-induced aggregates were less globular in morphology, the apparatus was still capable of stimulating synovial fluid aggregates at each concentration of synovial fluid. It is possible that the introduction of fluid flow might lower the bacterial concentrations required to stimulate aggregate formation, because it would enhance the probability of collisions.

As described previously, the synovial cavity following joint surgery is primarily filled with blood. Human blood is approximately twice as viscous as PBS and contains excess polymers within the serum and plasma components that may contribute to early aggregate formation (23, 24). To simulate the refilling of synovial fluid in the joint space, displacing the blood, we incubated *S. aureus* for 1 h on a shaker with various concentrations of synovial fluid and heparinized human blood. Although heparin is seldom used during surgery, patients are often placed on anticoagulants either the day of surgery or postoperatively. As expected, we noticed a degree of macroscopic aggregate formation in the 100% blood. Supplementation of either 10% BSF or 25% BSF into the blood produced comparably sized macroscopic aggregates. However, higher concentrations of synovial fluid with small amounts of blood diminished the large, globular aggregate phenotype. We suspect that, in combination with the blood, higher concentrations of synovial fluid create a system that is too viscous to facilitate aggregate formation, even under dynamic conditions. These data corroborate our hypothesis that early time points with lower synovial fluid concentrations may be optimal for aggregate formation. Interestingly, upon microscopic observation, our blood-10% synovial fluid aggregates displayed phenotypic similarity to synovial fluid aggregates observed in the synovial fluid of patients with infected joints (8). Our findings indicate not only that the presence of synovial fluid polymers is important for aggregate formation but also that their use by *S. aureus* is highly influenced by the state of the joint environment.

Following surgical site closure, there will likely be periods of both static and dynamic fluid conditions that stimulate the formation of distinct aggregate phenotypes. Therefore, we sought to understand the mechanics of synovial fluid-induced aggregation under both conditions. Because the presence of fibrinogen and fibronectin has been widely reported to be essential for aggregate formation in synovial fluid, we first tested whether direct bacterial interaction with these polymers was required to form both aggregate phenotypes. With the use of a fibronectin-binding protein and clumping factor quadruple mutant strain, we examined the necessity for key binding proteins in synovial fluid aggregate formation under both dynamic and static conditions.

While the mutant strain was capable of aggregating under static conditions to a degree, the macroscopic, free-floating aggregate phenotype was inhibited under dynamic conditions. These findings support our hypothesis that aggregation in synovial fluid is potentially a multistep process, with requirements changing under different joint conditions. While it is likely that the adhesin mutant strain is still capable of weakly binding these polymers using other binding factors, our observations indicate that they are insufficient for forming stable macroscopic aggregates under shear (25).

To directly assess the requirement for fibrinogen binding by the bacterial surface adhesins, microscopy and macroscopic imaging were conducted following both dynamic and static incubation with 0.2 mg/mL Alexa Fluor 488-conjugated human fibrinogen. In contrast to incubation in 10% BSF, the adhesin mutant was unable to form either a macroscopic aggregate under dynamic conditions or branched aggregates under static conditions, while fibrinogen was sufficient to stimulate both phenotypes under both conditions with the wild-type strain.

Interestingly, gentamicin-killed bacteria also aggregated upon contact with 10% BSF, indicating that active bacterial processes are not required for synovial fluid-induced aggregation to occur and the presence of the surface adhesins is sufficient. Unexpectedly, gentamicin-killed bacterial aggregates were on average 20% larger than the live bacteria in the untreated control. This may be due to changes in bacterial expression in response to antibiotic stress. It has been reported that, within 30 min of gentamicin exposure ($100\times$ the MIC), there is a significant elevation in the expression of SigB, a stress-responsive alternative sigma factor (26, 27). SigB activity positively influences the expression of clumping factors and fibronectin-binding

proteins, which could explain the increase in aggregation observed with the gentamicin-treated bacteria (28–30). Taken together, these findings confirm our speculation that bridging aggregation does occur through the rapid interaction of bacterial adhesins with fibrinogen, but they suggest that it is not the only contributor to the aggregate phenotype.

A possible explanation for our observation of static aggregation in 10% BSF but not fibrinogen alone is the capacity for the mutant to interact with or be influenced by other synovial fluid polymers, such as hyaluronic acid and albumin (31–34). Preliminary data show that bovine serum albumin (BSA) stimulates clumping in both the mutant and the wild-type strain. Furthermore, high-molecular-weight hyaluronic acid has been documented to facilitate depletion aggregation in *Pseudomonas aeruginosa*, yielding compact, aligned bacterial aggregates (19). The domination of the depletion mechanism in the absence of functional polymer bridging could explain the greater degree of circularity observed in the adhesin mutant aggregates, compared to the highly branched wild-type aggregates, following incubation in 10% BSF. We are currently evaluating each of these possibilities by use of synthetic synovial fluid to assess the influence of other host components on aggregate formation under each condition.

Synovial fluid-induced aggregation has recently been acknowledged as a potential contributor to the occurrence of orthopedic joint infections. Our basic understanding of aggregate formation in synovial fluid has grown exponentially over the past decade; however, future studies must include conditions that consider the infection environment. In the context of joint surgery, the infection environment is both dynamic and inflammatory, with fluctuating concentrations of blood, synovial fluid, and the polymers of which they are composed. We report here that changes in these factors significantly impact the extent and rapidity of synovial fluid-induced aggregation of *S. aureus*. Additionally, we observe that fluid dynamics may play a critical role in aggregation, potentially facilitating aggregate formation with smaller bacterial inocula and higher synovial fluid concentrations. In addition to assessing the influence of joint conditions on aggregate formation, our work provides evidence of a polymer bridging mechanism through interaction between key staphylococcal surface adhesins and fibrinogen. Because synovial fluid is a complex fluid, we hope to further tease apart the specific bacterial and host factors dictating aggregation in future studies.

MATERIALS AND METHODS

Bacterial strains and growth conditions. A methicillin-resistant *S. aureus* LAC strain expressing GFP (AH1726) was used for all confocal microscopy, image analysis quantification, and growth curves. For macroscopic imaging experiments, the quadruple mutant AH4413 ($\Delta clfA \Delta fnbAB clfB::Tn$) was utilized along with the wild-type strain, AH1263 (35). Cultures were streaked on tryptic soy agar (TSA) (BD Biosciences, Heidelberg, Germany) from agar slants (Horswill Laboratory, University of Colorado School of Medicine, Aurora, CO). TSA plates were incubated overnight at 37°C, and a single isolated colony was used to inoculate 5 mL of tryptic soy broth (TSB) (BD Biosciences) in a 15-mL Falcon tube. Inoculated broth cultures were grown for 18 h at 37°C in an orbital shaker set to 200 rpm (Innova 44; New Brunswick Scientific).

Confocal imaging of aggregates. Overnight cultures of AH1726 were grown as described previously and diluted to an optical density at 600 nm (OD_{600}) of 0.2. One milliliter of the diluted culture was pelleted at $21,000 \times g$ for 1 min in a centrifuge before resuspension in 1 mL of PBS. The cells were then transferred into a glass-bottomed confocal dish (35 by 10 mm; MatTek Corp., Ashland, MA) containing 2 mL of PBS or PBS supplemented with synovial fluid and/or hyaluronic acid. Confocal microscopy was conducted 1 h after bacterial incubation in PBS, 10% BSF in PBS, 20% BSF in PBS, or 50% BSF in PBS at room temperature. Additionally, the effect of viscosity on synovial fluid-induced aggregation was assessed by imaging 1 h after incubation in 10% BSF supplemented with increasing concentrations of high-molecular-weight hyaluronic acid sodium salt (1.5 to 1.8 MDa; Alfa Aesar, Haverhill, MA, USA) in PBS. The pH value was measured for each solution to ensure that pH was not influencing aggregation phenotypes (see Fig. S2 in the supplemental material). Fibrinogen aggregates were stimulated using 0.2 mg/mL purified fibrinogen from human plasma with an Alexa Fluor 488 conjugate (Invitrogen, Waltham, MA). Images were collected using an Olympus Fluoview FV10i confocal laser scanning microscope under $\times 60$ magnification with an additional $\times 2$ zoom. For each condition, 3 biological replicates were imaged, with 5 representative images being captured for each replicate.

Aggregate size quantification in Fiji. Following confocal imaging, green channel images displaying GFP-tagged synovial fluid-induced aggregates were imported into Fiji image analysis software (36). Replicates were converted from individual images to stacks for batch processing. The TIFF stacks were converted to 8-bit images, and a threshold was applied using an autothreshold. Size threshold detection was set to include particles ≥ 9.6 pixels or $1 \mu\text{m}$ in diameter, excluding background particles that were smaller than a single bacterial cell. Particles were analyzed, and the average particle size for each image was calculated. Size data were transferred to Prism GraphPad for graphing and statistical analysis. For the synovial fluid concentrations and viscosity experiments, statistical significance was determined by one-way analysis of variance (ANOVA) followed by

Bonferroni's multiple-comparison test to compare means between treatments. To determine whether the relationship between time and aggregate size was statistically significant, a linear regression analysis was performed and an R^2 value was calculated.

Aggregate skeletonization and branching analysis. As described above, the green channel images displaying GFP-tagged aggregates were imported into Fiji image analysis software for branching quantification. The TIFF stacks were first converted to 8-bit images and made binary for skeletonization (37). Binary images were skeletonized to display branching structures for each aggregate. The size threshold detection was set to include only particles ≥ 9.6 pixels ($1 \mu\text{m}$) in diameter, excluding background particles that were smaller than a single bacterial cell. All branch lengths were quantified for each image and exported to Excel. The 50 longest branches for each image were averaged and transferred to Prism for graphing and statistical analysis. For the synovial fluid concentration data and viscosity experiments, statistical significance was determined by one-way ANOVA followed by Bonferroni's multiple-comparison test to compare means between treatments. To determine whether the relationship between time and aggregate branch length was statistically significant, a linear regression analysis was performed and an R^2 value was calculated.

Macroscopic imaging of dynamic aggregates. Macroscopic analysis of the dynamically formed aggregates was carried out as described in a previous work (38). The GFP-expressing *S. aureus* strain AH1726 was grown overnight as described above and subsequently diluted to an OD_{600} of 0.5. The bacteria were pelleted, and the supernatant was aspirated before resuspension in 1 mL of PBS. The 1 mL of bacteria was transferred to a 35- by 10-mm petri dish and supplemented with either 1.7 mL, 1.4 mL, or 500 μL of additional PBS. Finally, 300 μL , 600 μL , or 1,500 μL of BSF supernatant was added to create 10% BSF, 20% BSF, or 50% BSF in PBS solutions, respectively. The petri dishes were incubated for 1 h at room temperature on an orbital shaker set to 60 rpm. The same conditions were used to evaluate aggregate formation on a rocker, which we suspect more closely resembles dynamic movement in a joint cavity. Following a 1-h incubation on either apparatus, macroscopic imaging was conducted using a dual 12-megapixel camera secured 15 cm above the specimen. In addition to PBS, macroscopic imaging was conducted following incubation in synovial fluid-supplemented human blood. Human blood was isolated from a healthy donor by intravenous puncture following an institutional review board (The Ohio State University)-approved protocol (protocol number: 2009H0314). Pelleted bacteria were diluted to an OD_{600} of 0.5 and resuspended in blood supplemented with increasing concentrations of BSF.

Statistical analysis. GraphPad Prism v9.20 software was used for statistical analysis of the following data. The threshold significance was set at a P value of 0.05. All error bars indicate the standard error of the mean (SEM). Statistically significant differences were determined using the tests specified in the descriptions.

SUPPLEMENTAL MATERIAL

Supplemental material is available online only.

VIDEO S1, AVI file, 5.6 MB.

VIDEO S2, AVI file, 4.3 MB.

VIDEO S3, AVI file, 4.2 MB.

TEXT S1, DOCX file, 0.01 MB.

FIG S1, TIF file, 0.3 MB.

FIG S2, TIF file, 0.2 MB.

FIG S3, TIF file, 1.1 MB.

ACKNOWLEDGMENTS

A.S. was supported by the Ohio State University College of Medicine (Program for Advancing Research in Infection and Immunity Fellowship). P.S. is supported by NIH grant R01 GM124436. A.R.H. is supported by NIH grant AI083211.

REFERENCES

1. Pestrak MJ, Gupta TT, Dusane DH, Guzior DV, Staats A, Harro J, Horswill AR, Stoodley P. 2020. Investigation of synovial fluid induced *Staphylococcus aureus* aggregate development and its impact on surface attachment and biofilm formation. *PLoS One* 15:e0231791. <https://doi.org/10.1371/journal.pone.0231791>.
2. Gupta TT, Gupta NK, Pestrak MJ, Dusane DH, Harro JM, Horswill AR, Stoodley P. 2020. *Staphylococcus aureus* aggregates on orthopedic materials under varying levels of shear stress. *Appl Environ Microbiol* 86:e01234-20. <https://doi.org/10.1128/AEM.01234-20>.
3. Gilbertie JM, Schnabel LV, Hickok NJ, Jacob ME, Conlon BP, Shapiro IM, Parvizi J, Schaer TP. 2019. Equine or porcine synovial fluid as a novel ex vivo model for the study of bacterial free-floating biofilms that form in human joint infections. *PLoS One* 14:e0221012. <https://doi.org/10.1371/journal.pone.0221012>.
4. Knott S, Curry D, Zhao N, Metgud P, Dastgheyb SS, Purtill C, Harwood M, Chen AF, Schaer TP, Otto M, Hickok NJ. 2021. *Staphylococcus aureus* floating biofilm formation and phenotype in synovial fluid depends on albumin, fibrinogen, and hyaluronic acid. *Front Microbiol* 12:655873. <https://doi.org/10.3389/fmicb.2021.655873>.
5. Perez K, Patel R. 2015. Biofilm-like aggregation of *Staphylococcus epidermidis* in synovial fluid. *J Infect Dis* 212:335–336. <https://doi.org/10.1093/infdis/jiv096>.
6. Staats A, Li D, Sullivan AC, Stoodley P. 2021. Biofilm formation in periprosthetic joint infections. *Ann Joint* 6:43. <https://doi.org/10.21037/aoj-20-85>.
7. Burel C, Dreyfus R, Purevdorj-Gage L. 2021. Physical mechanisms driving the reversible aggregation of *Staphylococcus aureus* and response to antimicrobials. *Sci Rep* 11:15048. <https://doi.org/10.1038/s41598-021-94457-1>.
8. Bidossi A, Bottagisio M, Savadori P, De Vecchi E. 2020. Identification and characterization of planktonic biofilm-like aggregates in infected synovial fluids from joint infections. *Front Microbiol* 11:1368. <https://doi.org/10.3389/fmicb.2020.01368>.

9. McCarty WJ, Luan A, Siddiqui M, Hansen BC, Masuda K, Sah RL. 2011. Biomechanical properties of mixtures of blood and synovial fluid. *J Orthop Res* 29:240–246. <https://doi.org/10.1002/jor.21209>.
10. Greenwald RA, Moak SA. 1986. Degradation of hyaluronic acid by polymorphonuclear leukocytes. *Inflammation* 10:15–30. <https://doi.org/10.1007/BF00916037>.
11. Seidman AJ, Limaiem F. 2021. Synovial fluid analysis. StatPearls Publishing LLC, Treasure Island, FL.
12. Baker MS, Green SP, Lowther DA. 1989. Changes in the viscosity of hyaluronic acid after exposure to a myeloperoxidase-derived oxidant. *Arthritis Rheum* 32:461–467. <https://doi.org/10.1002/anr.1780320416>.
13. Boff D, Crijns H, Teixeira MM, Amaral FA, Proost P. 2018. Neutrophils: beneficial and harmful cells in septic arthritis. *Int J Mol Sci* 19:468. <https://doi.org/10.3390/ijms19020468>.
14. Gupta RC, Lall R, Srivastava A, Sinha A. 2019. Hyaluronic acid: molecular mechanisms and therapeutic trajectory. *Front Vet Sci* 6:192. <https://doi.org/10.3389/fvets.2019.00192>.
15. Tamer TM. 2013. Hyaluronan and synovial joint: function, distribution and healing. *Interdiscip Toxicol* 6:111–125. <https://doi.org/10.2478/intox-2013-0019>.
16. LeBoeuf RD, Gregg RR, Weigel PH, Fuller GM. 1987. Effects of hyaluronic acid and other glycosaminoglycans on fibrin polymer formation. *Biochemistry* 26:6052–6057. <https://doi.org/10.1021/bi00393a016>.
17. Faryna A, Goldenberg K. 1990. Chapter 166. Joint fluid. In Walker HK, Hall WD, Hurst JW (ed), *Clinical methods: the history, physical, and laboratory examinations*, 3rd ed. Butterworths, Boston, MA.
18. Berezkin AG. 1978. Time required for replenishment of synovial fluid under experimental conditions. *Arkh Anat Gistol Embriol* 75:86–90. (In Russian).
19. Secor PR, Michaels LA, Ratjen A, Jennings LK, Singh PK. 2018. Entropically driven aggregation of bacteria by host polymers promotes antibiotic tolerance in *Pseudomonas aeruginosa*. *Proc Natl Acad Sci U S A* 115:10780–10785. <https://doi.org/10.1073/pnas.1806005115>.
20. McCarty WJ, Masuda K, Sah RL. 2011. Fluid movement and joint capsule strains due to flexion in rabbit knees. *J Biomech* 44:2761–2767. <https://doi.org/10.1016/j.jbiomech.2011.09.005>.
21. Lenssen TAF, van Steyn MJA, Crijns YHF, Waltjé EMH, Roos GM, Geesink RJT, van den Brandt PA, De Bie RA. 2008. Effectiveness of prolonged use of continuous passive motion (CPM), as an adjunct to physiotherapy, after total knee arthroplasty. *BMC Musculoskelet Disord* 9:60. <https://doi.org/10.1186/1471-2474-9-60>.
22. Jungblut S, Joswig JO, Eychmüller A. 2019. Diffusion- and reaction-limited cluster aggregation revisited. *Phys Chem Chem Phys* 21:5723–5729. <https://doi.org/10.1039/c9cp00549h>.
23. Yeom E, Kang YJ, Lee SJ. 2014. Changes in velocity profile according to blood viscosity in a microchannel. *Biomicrofluidics* 8:034110. <https://doi.org/10.1063/1.4883275>.
24. Nader E, Skinner S, Romana M, Fort R, Lemonne N, Guillot N, Gauthier A, Antoine-Jonville S, Renoux C, Hardy-Dessources MD, Stauffer E, Joly P, Bertrand Y, Connes P. 2019. Blood rheology: key parameters, impact on blood flow, role in sickle cell disease and effects of exercise. *Front Physiol* 10:1329. <https://doi.org/10.3389/fphys.2019.01329>.
25. Josse J, Velard F, Gangloff SC. 2015. *Staphylococcus aureus* vs. osteoblast: relationship and consequences in osteomyelitis. *Front Cell Infect Microbiol* 5:85. <https://doi.org/10.3389/fcimb.2015.00085>.
26. Kubistova L, Dvoracek L, Tkadlec J, Melter O, Licha I. 2018. Environmental stress affects the formation of *Staphylococcus aureus* persists tolerant to antibiotics. *Microb Drug Resist* 24:547–555. <https://doi.org/10.1089/mdr.2017.0064>.
27. Rodriguez Ayala F, Bartolini M, Grau R. 2020. The stress-responsive alternative sigma factor SigB of *Bacillus subtilis* and its relatives: an old friend with new functions. *Front Microbiol* 11:1761. <https://doi.org/10.3389/fmicb.2020.01761>.
28. Entenza JM, Moreillon P, Senn MM, Kormanec J, Dunman PM, Berger-Bächi B, Projan S, Bischoff M. 2005. Role of σ B in the expression of *Staphylococcus aureus* cell wall adhesins ClfA and FnbA and contribution to infectivity in a rat model of experimental endocarditis. *Infect Immun* 73:990–998. <https://doi.org/10.1128/IAI.73.2.990-998.2005>.
29. Marbach H, Mayer K, Vogl C, Lee JYH, Monk IR, Sordelli DO, Buzzola FR, Ehling-Schulz M, Grunert T. 2019. Within-host evolution of bovine *Staphylococcus aureus* selects for a SigB-deficient pathotype characterized by reduced virulence but enhanced proteolytic activity and biofilm formation. *Sci Rep* 9:13479. <https://doi.org/10.1038/s41598-019-49981-6>.
30. Burian M, Plange J, Schmitt L, Kaschke A, Marquardt Y, Huth L, Baron JM, Hornef MW, Wolz C, Yazdi AS. 2021. Adaptation of *Staphylococcus aureus* to the human skin environment identified using an ex vivo tissue model. *Front Microbiol* 12:728989. <https://doi.org/10.3389/fmicb.2021.728989>.
31. Navarre WW, Schneewind O. 1999. Surface proteins of Gram-positive bacteria and mechanisms of their targeting to the cell wall envelope. *Microbiol Mol Biol Rev* 63:174–229. <https://doi.org/10.1128/MMBR.63.1.174-229.1999>.
32. Ibberson CB, Parlet CP, Kwiecinski J, Crosby HA, Meyerholz DK, Horswill AR. 2016. Hyaluronan modulation impacts *Staphylococcus aureus* biofilm infection. *Infect Immun* 84:1917–1929. <https://doi.org/10.1128/IAI.01418-15>.
33. Pigman W, Gramling E, Holley HL. 1961. Interactions of hyaluronic acid with serum albumin. *Biochim Biophys Acta* 46:100–107. [https://doi.org/10.1016/0006-3002\(61\)90651-5](https://doi.org/10.1016/0006-3002(61)90651-5).
34. Cheng AG, Missiakas D, Schneewind O. 2014. The giant protein Ehb is a determinant of *Staphylococcus aureus* cell size and complement resistance. *J Bacteriol* 196:971–981. <https://doi.org/10.1128/JB.01366-13>.
35. Boles BR, Thoende M, Roth AJ, Horswill AR. 2010. Identification of genes involved in polysaccharide-independent *Staphylococcus aureus* biofilm formation. *PLoS One* 5:e10146. <https://doi.org/10.1371/journal.pone.0010146>.
36. Schindelin J, Arganda-Carreras I, Frise E, Kaynig V, Longair M, Pietzsch T, Preibisch S, Rueden C, Saalfeld S, Schmid B, Tinevez JY, White DJ, Hartenstein V, Eliceiri K, Tomancak P, Cardona A. 2012. Fiji: an open-source platform for biological-image analysis. *Nat Methods* 9:676–682. <https://doi.org/10.1038/nmeth.2019>.
37. Arganda-Carreras I, Fernández-González R, Muñoz-Barrutia A, Ortiz-Del-Solozano C. 2010. 3D reconstruction of histological sections: application to mammary gland tissue. *Microsc Res Tech* 73:1019–1029. <https://doi.org/10.1002/jemt.20829>.
38. Staats A, Burbach PW, Eltobgy M, Parker DM, Amer AO, Wozniak DJ, Wang S-H, Stevenson KB, Urish KL, Stoodley P. 2021. Synovial fluid-induced aggregation occurs across *Staphylococcus aureus* clinical isolates and is mechanistically independent of attached biofilm formation. *Microbiol Spectr* 9:e0026721. <https://doi.org/10.1128/Spectrum.00267-21>.